Dyes and Pigments 185 (2021) 108951

Contents lists available at ScienceDirect

Dyes and Pigments

journal homepage: http://www.elsevier.com/locate/dyepig

Effect of thiophene-based π-spacers on *N*-arylphenothiazine dyes for dye-sensitized solar cells

David Moe Almenningen [a], Henrik Erring Hansen [b], Martin Furru Vold [a], Audun Formo Buene [a], Vishwesh Venkatraman [a], Svein Sunde [b], Bård Helge Hoff [a], Odd Reidar Gautun [a,*]

[a] Department of Chemistry, Norwegian University of Science and Technology, Høgskoleringen 5, NO-7491, Trondheim, Norway
[b] Department of Materials Science and Engineering, Norwegian University of Science and Technology, Sem Sælands Vei 12, NO-7491, Trondheim, Norway

ARTICLE INFO

Keywords:
Oligothiophene
Phenothiazine dye
Dye-sensitized solar cell
π-spacer
Electrochemical impedance spectroscopy

ABSTRACT

To study the effect of π-spacers on dye performance in DSSC, five novel phenothiazine dyes have been prepared where the number of successive thiophenes in the π-spacer was increased from zero to four. Additionally, a dye bearing thieno[3,2-*b*]thiophene was synthesized, and compared to its unfused bithiophene analogue. When the number of thiophenes were two or more the light absorption properties was significantly better in the region 400–550 nm compared to the dye without a π-spacer. DSSC device testing revealed that the reference dye without a π-spacer gave the best overall performance producing a power conversion efficiency of 5.7% (J_{SC} = 10.1 mA cm^{-2}, V_{OC} = 0.83 V, FF = 0.68), attributed to the superior V_{OC} of this dye. The incorporation of one and two thiophenes resulted in a similar performance as the reference, while incorporation of larger oligothiophenes proved to be deleterious to DSSC-performance. Electrochemical impedance spectroscopy indicates that the voltage drops and performance loss associated with these dyes are due to more facile recombination.

1. Introduction

The nascence of dye-sensitized solar cells (DSSC), brought on by O'Regan and Grätzel in 1991, established a novel photovoltaic technology with unique and promising properties [1]. Traits such as their transparency make DSSC interesting for building integrated photovoltaics (BIPV) [2], they can be made using flexible materials allowing them to be integrated on cloth and wearable devices [3], and their power conversion efficiency under low-light conditions exceed that of the established GaAs solar cells proving their viability for low-power applications [4]. Moreover, Hardin et al. estimate that a competitive price of US$0.20–0.30 W^{-1} can be achieved [5], which is an additional driving force for continued research in this field.

Fully organic dyes for DSSC vary greatly in chemical structure, but most of them adopt some variety of a D-π-A structural motif. Such molecules are constituted of an electron rich donor (D), a π-conjugated linker (π), and an electron acceptor (A) [6]. This architecture facilitates a charge separation upon excitation where electron density is moved from the donor part to the acceptor. Through molecular engineering of the dye structure it is possible to customize the properties of the chromophore. It has been shown that increasing the electron donor properties raise the energy level of the highest occupied molecular orbital (HOMO), and red-shift the absorption maxima [7–9]. Likewise, it has been shown that stronger electron acceptors also red-shift the UV/Vis adsorption [10], as this will also ensure an efficient internal charge transfer (ICT). For a thorough review of property tuning in D-π-A molecules the reader is referred to the comprehensive paper by Bureš on the topic [11].

The research on new dyes for DSSC has led to an enormous amount of papers on optimizing the different parts of the D-π-A molecule. The only part that is seemingly optimized is the acceptor side, where cyanoacrylic acid is by far the most widely used anchoring group due to its strong electron withdrawing properties as well as the acidic group that binds the dye to TiO_2 [12]. There is no clear consensus on the donor. However, triphenylamine-derivatives have displayed good photovoltaic properties in numerous reports [4,13,14]. With regards to the π-linker a number of promising and different candidates have been synthesized and assessed [15–18]. A DSSC co-sensitized by two fully organic dyes (ADEKA-1 and LEG4 see Fig. 1) offer the highest achieved PCE so far at 14.3% [19]. Both of these record dyes are equipped with a thiophene-based linker. Incorporation of thiophene has proven to be useful in broadening the spectral response of chromophores compared to the reference dyes without π-linkers [20,21]. Expanding from thiophene

* Corresponding author.
E-mail address: odd.r.gautun@ntnu.no (O.R. Gautun).

https://doi.org/10.1016/j.dyepig.2020.108951
Received 17 September 2020; Received in revised form 20 October 2020; Accepted 20 October 2020
Available online 23 October 2020

to oligothiophenes further broadens the spectral response as revealed by studies of different donors like coumarin [22], phenothiazine [23], benzo[a]carbazole [24], and triphenylamine [25,26].

A downside of this strategy is the observed drop in photovoltage [22,26]. Two explanations has been offered for this phenomenon, (i) the electrostatic and charge transfer effect of longer oligothiophenes downshift the conduction band of TiO_2 [27] (ii) the sulfur atom of thiophene and iodine components in the electrolyte interact and form dye-iodine complexes [28]. Ronca et al. performed a theoretical study on a set of known sensitizers [27]. They discovered that significant charge-rearrangement occurred at the dye-titania interface, and demonstrated that longer π-linkers were associated with less efficient charge transfer, leading to a downshift of the conduction band of TiO_2 and a subsequent drop in V_{OC}. This is supported by the work of Rühle et al. who demonstrated that the dipole moment of molecules adsorbed onto TiO_2 had a profound impact on V_{OC} [29]. They found that molecules with a dipole moment pointing away from the TiO_2 surface lowered the energy of the conduction band, decreasing the difference between E_{CB} and E_{redox}. Furthermore the sulfur-iodine interaction theory is supported by the work of Zhang et al., which showed that longer oligothiophenes had a higher probability of forming dye-iodine complexes [28]. Such a phenomenon would accumulate electrolyte species near the titania surface, facilitating recombination at the TiO_2-electrolyte interface. This probably explains why longer oligothiophenes demonstrate higher photovoltages than shorter ones in cobalt-based electrolyte systems, as opposed to the traditional iodine electrolyte [28,30].

Thiophene-derivatives have demonstrated their suitability as π-linkers in organic dyes for DSSC. The most striking example is the co-sensitization of **LEG4** and **ADEKA-1** which led to the current PCE-record for DSSCs, at 14.3% [19], see Fig. 1. The series **T1-T4**, presented by Liu and coworkers, showed that the PCE-values could be improved through increasing the size of the oligothiophene π-spacer [26]. Our previous work on π-linkers revealed only marginal performance increase using a furan spacer (**AFB-11** in Fig. 1), while the other spacers in the study (**AFB-3**,**-5**,**-7**, and **-9**), including thiophene, showed lower efficiency than the reference dye without a π-linker [20]. In view of these conflicting results, we wished to investigate whether longer oligothiophenes can generate sufficiently high photocurrents to offset the associated loss of photovoltage. We have based our comparison on the series of six novel dyes, as shown in Fig. 1. These include one reference dye (**DMA-0**) without any π-spacer. Four dyes (**DMA-1 – DMA-4**) where the π-linker is increased from one to four consecutive 2,5-linked thiophenes. (The dyes **DMA-0 – DMA-4** are named after the number of thiophenes in the π-spacer). Additionally, one dye was synthesized (**DMA-5**) with a rigidified thieno[3,2-*b*]thiophene and also tested.

2. Results and discussion

2.1. Dye synthesis

The dyes in the series all bear the same phenothiazine donor. The hexyloxyphenyl moiety was chosen as the amine substituent to reduce aggregation of the dyes, as this group has been used successfully in previously reported phenothiazine dyes [32,33]. The auxiliary donor chosen for this study was 2,4-dipropoxyphenyl, which was easily introduced by its commercially available boronic acid. The analogous 2,4-dibutoxyphenyl moiety has proven to be an effective auxiliary donor for triphenylamine dyes [15,34].

The synthesis of the reference dye **DMA-0** was performed through the route shown in Scheme 1. The starting material **1** was prepared according to literary procedures [35,36]. The following two steps of the synthesis were also carried out through a previously reported procedure [37], giving the building block **3** in 53% yield over two steps. The

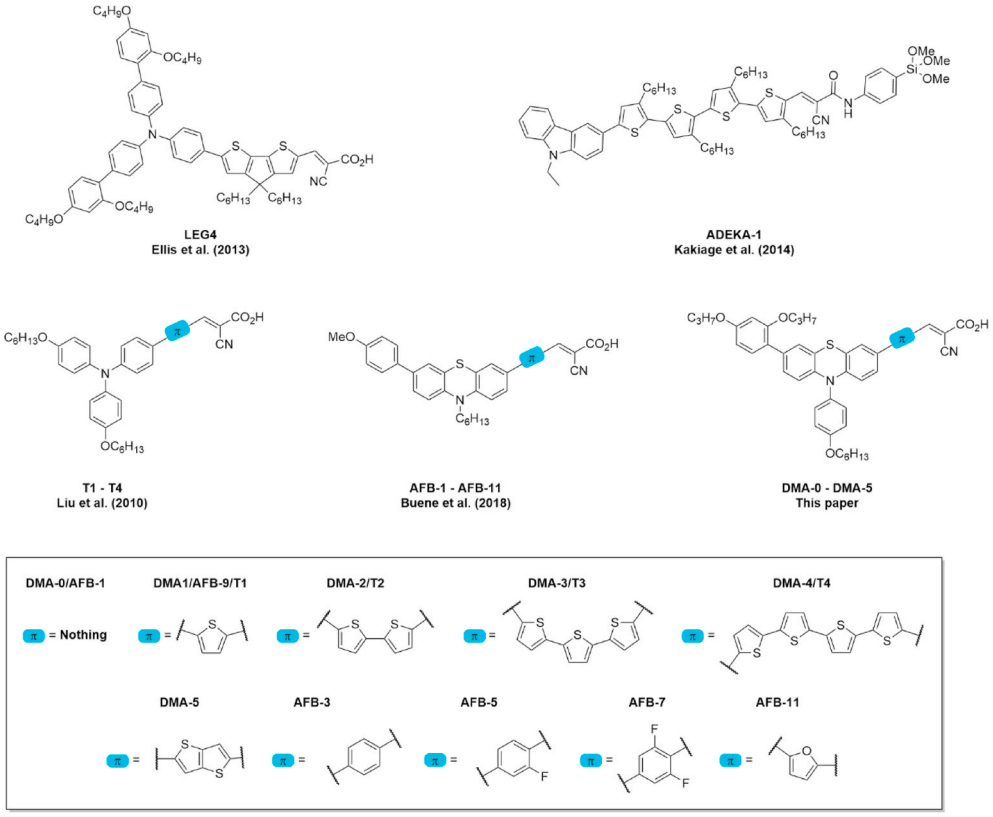

Fig. 1. An assortment of previously synthesized dyes, and the novel dyes presented herein. The dye **LEG4** [15] and **ADEKA-1** [31] are examples of successful dyes employing thiophene-derivatives in the π-spacer. The series **T1-T4** [26] are furnished with increasingly sized oligothiophenes. The π-spacer of **AFB-1 – AFB-11** is varied from nothing to six-membered aromatics to five-membered heteroaromatics.

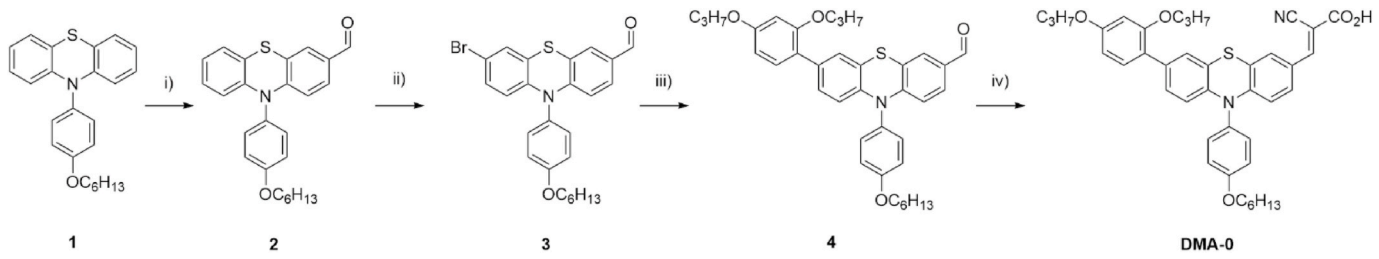

Scheme 1. Synthesis route for the reference dye **DMA-0**. i) $POCl_3$, DMF, ii) NBS, iii) $Pd(OAc)_2$, SPhos, K_3PO_4, (2,4-dipropoxyphenyl)boronic acid, iv) cyanoacetic acid, piperidine.

brominated phenothiazine was then functionalized with an auxiliary donor through a Suzuki-Miyaura reaction. Following the Knoevenagel condensation procedure reported by Iqbal et al. [21] the cyano-acrylic acid anchor was installed, producing the dye **DMA-0** in a satisfactory yield of 88%.

A selective mono-bromination of **1** using NBS (Scheme 2), allowed for the installment of the 2,4-dipropoxyphenyl auxiliary donor in a subsequent Suzuki-Miyaura cross-coupling. A three-step procedure from **6** to the aldehydes **7**–**11** was utilized. The first step was a bromination, then a borylation using a procedure described by Billingsley and Buchwald [38] produced the pinacol boronate ester. This was used further in a Suzuki-Miyaura cross-coupling with brominated thiophene carbaldehydes to yield the dye-precursors **7**–**11** in yields of ~20–40% over three steps. The aforementioned Knoevenagel procedure was employed once more to yield the target dyes **DMA-1 - DMA-5** in yields of 64–97%. The specific synthetic procedures are found in the ESI.

2.2. Photophysical properties

The spectral response of the dyes was studied in solution (DCM, 2×10^{-5} M, Fig. 2), and while adsorbed onto TiO_2 films (Fig. 3). The data from these experiments are summarized in Table 1. Surprisingly, the reference dye **DMA-0**, without any π-spacer, displayed the second-most redshifted absorption maxima of the dyes in solution (Fig. 2), albeit at the lowest molar extinction coefficient. A blueshift of the absorption maximum by 42 nm, was observed when introducing a thiophene π-linker in **DMA-1**. A similar, although much smaller, hypsochromic shift has been observed in our previous work, where a 4 nm reduction was observed [20].

When comparing the absorption maxima of the dyes in solution versus the dyes loaded on TiO_2-films, a 20–50 nm blueshift was seen for all the dyes. This could be caused by unfavorable dye-aggregation when the dyes were bound to titania [39], as no co-adsorbent CDCA was used for these measurements. Additionally, deprotonation of the dyes also causes blueshift of absorption [40], as shown in Fig. 4. For the reference dye **DMA-0**, the absorption spectrum of the carboxylate is in good accordance with the spectra from the TiO_2 film. For **DMA-4** a negligible shift of absorption maximum is seen in the spectrum of the carboxylate. This suggest that there are two different causes for the blueshift seen on TiO_2-films for these two dyes. The blueshift of **DMA-0** is largely attributed to deprotonation, meanwhile aggregation is responsible for the blueshift of **DMA-4.** For the remaining dyes in the series there seem to be a combination of these effects causing the blueshifts seen on the TiO_2 films. As shown in ESI Fig. S1, deprotonation of the dyes blueshift the dyes, but not to the same extent as seen when sensitized on TiO_2.

Extending the π-linker beyond one thiophene-unit redshifted the adsorption maxima for all the dyes in this series. For **DMA-2** a 48 nm redshift was seen (Fig. 2). A distinctly higher absorption in the region 400–550 nm was seen for the dyes bearing two or more thiophenes. A similar trend was seen when we investigated the absorption properties in THF, shown in ESI Fig. S2. As all the sensitizers bear the same donor- and acceptor-moieties, this effect is likely to be explained by the higher conjugation. For the dyes absorbed onto TiO_2 this effect was also present, where all the longer oligothiophene dyes displayed better adsorption properties than **DMA-1**. Care should be given with regards to these results, however, as small differences in film thickness as well as dye-loading will affect the absorption measurements.

The optical band gaps were estimated by the intersection of the absorption and normalized emission spectra. The reference dye, **DMA-0**, displayed the lowest band gap of the dyes synthesized, suggesting that

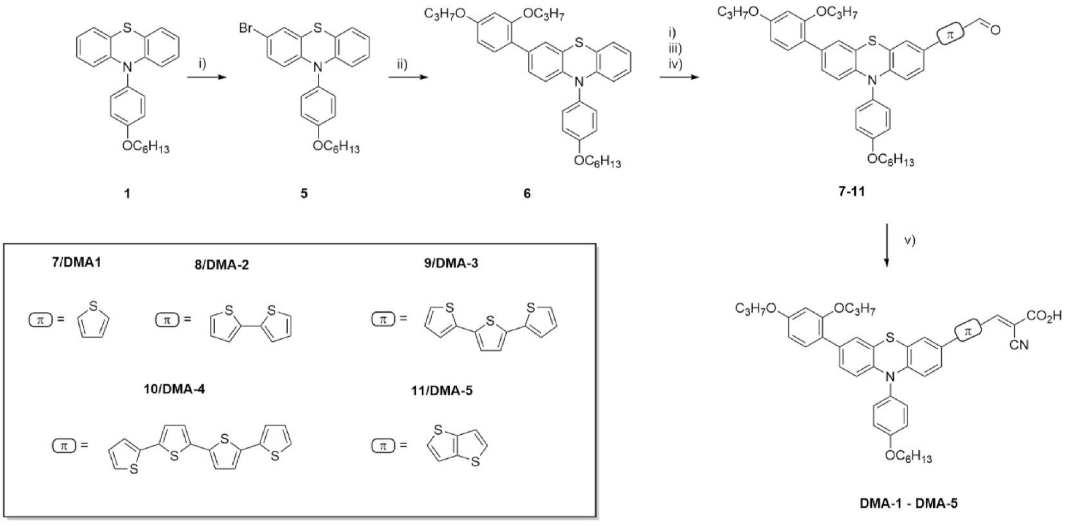

Scheme 2. Synthesis route for the thiophene-containing dyes **DMA-1 – DMA-5**. i) NBS, ii) $Pd(OAc)_2$, SPhos, K_3PO_4, (2,4-dipropoxyphenyl)boronic acid, iii) $PdCl_2(CH_3CN)_2$, SPhos, Et_3N, pinacol borane, iv) $Pd(OAc)_2$, SPhos, K_3PO_4, bromo-(thiophene)$_n$ carbaldehyde v) cyanoacetic acid, piperidine.

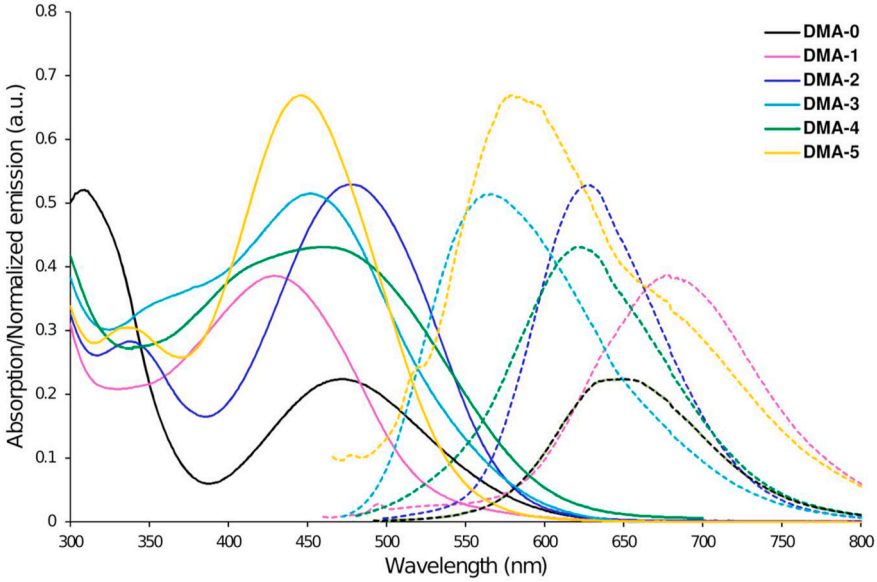

Fig. 2. Absorption and normalized emission spectra of all dyes in DCM solution.

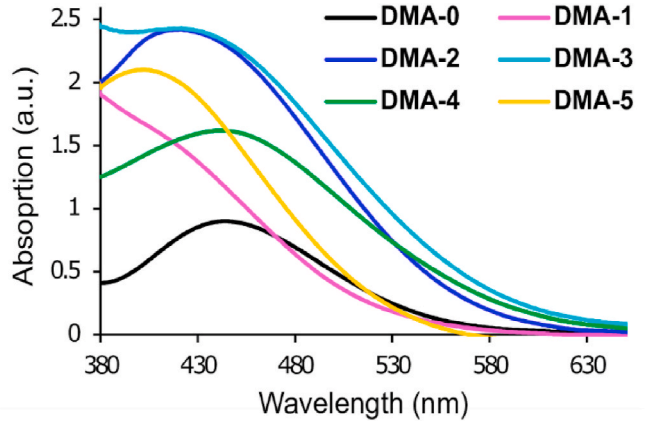

Fig. 3. UV/vis measurements of all dyes on TiO_2 films (2.5 μm, 18NR-T, Greatcell Solar).

incorporation of theses π-linkers are negatively affecting the ICT-process of the sensitizers. It is also noteworthy that the terthiophene linker of **DMA-3** increased the band gap significantly, while the band gap of the even larger quaterthiophene-bearing dye, **DMA-4,** was only moderately increased compared to the reference.

2.3. Electrochemical properties

An examination of the frontier orbital energies of **DMA-0** – **DMA-5** was carried out through cyclic voltammetry experiments. The working electrode was a stained TiO_2 electrode on FTO, and the counter electrode was a graphite carbon rod. A Ag/AgCl reference electrode was employed with supporting electrolyte 0.1 M LiTFSI in acetonitrile. The oxidation potential of all the dyes was measured vs F_c^+/F_c, and converted to vs. SHE by 0.624 V as reported by Pavlishchuk and Addison [41]. The recorded CVs are shown in ESI Fig. S3.

The deepest HOMO-level was seen for the reference dye **DMA-0** at 1.04 V vs. SHE (Fig. 5). Introduction of a thiophene π-spacer in dye **DMA-1** elevated the HOMO by 110 mV. This is consistent with previously reported phenothiazine dyes where even a 210 mV increase has been observed [42,43]. Similar HOMO-levels of the dyes was expected for a series of dyes bearing the same donor moiety, while the LUMO-levels of the dyes varied a lot with the different π-spacers.

Table 1
Photophysical and electrochemical properties of dyes in the series.

Dye	λ_{abs} [a] (nm)	ε ($M^{-1}cm^{-1}$)	Em. [b] (nm)	λ_{abs} [c] on TiO_2 (nm)	$E_{0\text{-}0}$ [d] (eV)	E_{ox} [e] (V vs SHE)	E_{LUMO} [f] (V)
DMA-0	472	11200	647	444	2.14	1.04	−1.10
DMA-1	430	19300	684	379	2.23	0.93	−1.30
DMA-2	478	26300	632	421	2.18	0.95	−1.23
DMA-3	452	25750	569	419	2.38	0.96	−1.42
DMA-4	461	21550	625	441	2.21	0.92	−1.29
DMA-5	446	33450	587	402	2.40	0.92	−1.48

[a] Maximum of most red-shifted peak.
[b] Emission when ICT band is excited, in DCM solution.
[c] Maximum of most red-shifted peak on TiO_2 (2.5 μm, GreatcellSolar 18NR-T).
[d] Calculated from the intersection of the absorption and normalized emission spectra.
[e] Measured vs. F_c^+/F_c on stained TiO_2 electrodes in acetonitrile with 0.1 M LiTFSI, converted to V vs. SHE by 0.624 V. Scan rate 10 mV s^{-1}.
[f] Calculated from E_{ox}-$E_{0\text{-}0}$.

The dyes synthesized in this study all displayed sufficiently deep HOMO-levels to be regenerated by the classic iodine redox shuttle. Unfortunately, only one of the dyes reported herein (**DMA-0**) had a sufficiently deep HOMO-level to be comfortably regenerated by the desirable Cu-electrolytes with redox potentials around 0.90 V vs SHE [44].

2.4. Theoretical calculations

Time-dependent density functional theory calculations (TD-DFT) was used to elucidate the electronic properties of the dyes reported herein. Calculations were performed using Gaussian 09 at the CAM-B3LYP/6-31G(d,p) level of theory [45]. The electron distribution of HOMO and LUMO for the two extremes (**DMA-0** and **DMA-4**) is shown in Fig. 6, the remaining dyes are shown in ESI Fig. S4. It was found that

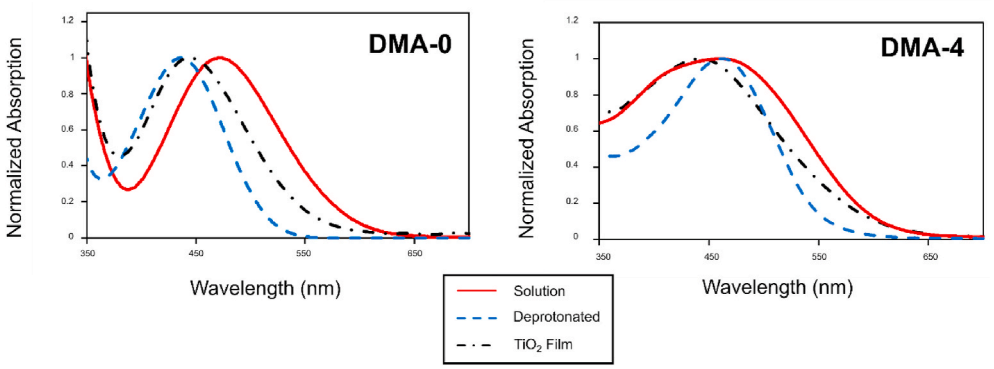

Fig. 4. UV/vis measurements of **DMA-0** and **DMA-4** in solution (DCM), deprotonated in solution, and sensitized on TiO_2 films. Deprotonation was carried out by adding a drop of triethylamine to the cuvette.

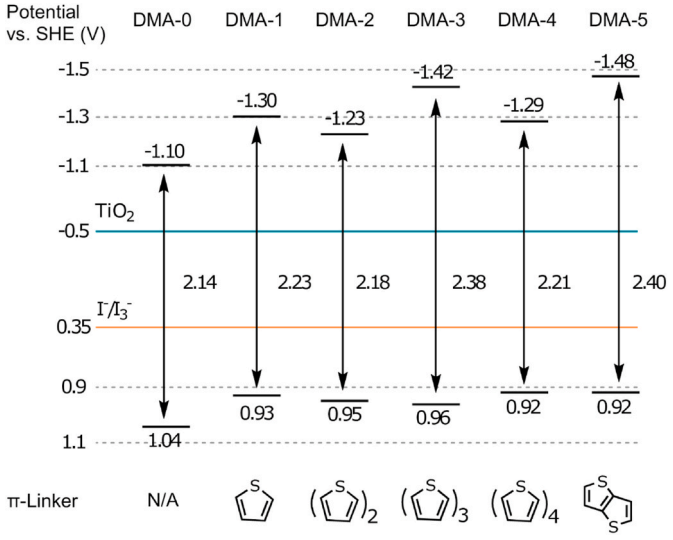

Fig. 5. Energy levels of the frontier orbitals for the sensitizers in this study.

the HOMO is largely located on the phenothiazine-core and the adjacent thiophene-unit for **DMA-1** – **DMA-4**. The LUMOs are found over the cyanoacrylic acid and the thiophenes close to the acceptor. This shows that excitation of the dye molecules moves the electron densities from phenothiazine to the acceptor moiety. This separation of electrons is associated with efficient injection of electron from the acceptor part of the dye to titania.

2.5. Photovoltaic properties

The photovoltaic performance of the dyes was characterized by fabricating three parallel DSSC-devices sensitized with each of the dyes, in addition a **N719** standard for reference. The results are presented in Table 2. The *J-V* curves of the fabricated DSSCs were measured under 1 sun AM 1.5 G illumination, and the best performing parallel was subjected to IPCE-measurements (Fig. 7 and Fig. 8). Integration of the IPCE-spectra over the 1 sun AM 1.5 G spectrum produced theoretical current densities within 20% of what was measured experimentally for all the sensitizers except **DMA-5**. This dye fell narrowly outside the criterion of reasonable correlation proposed by Christians et al. for the field of perovskite solar cells [46].

As also seen in our previous study on the effect of π-linkers on phenothiazine dyes, the reference dye without any spacers performed surprisingly well [20]. In this study **DMA-0** achieved the highest PCE largely owing to its excellent photovoltage with the I^-/I_3^- redox electrolyte. An expected photocurrent increase was seen for the iterative expansion of the oligothiophene moiety in **DMA-1** – **DMA-3**, ultimately achieving a J_{SC} of 11.01 mA/cm^2. To the authors surprise **DMA-4** did not produce a further increase in photocurrent, instead a significant drop in photovoltaic performance was observed. In a similar study, conducted by Liu et al., a series of dyes with a triphenylamine donor produced an ever increasing J_{SC} by increasing the number of thiophenes in the π-linker [26]. However, an increasingly sized aromatic system is more prone to detrimental aggregation effects, which could explain the lackluster J_{SC} of the quaterthiophene dye.

The voltage drops displayed by the thiophene-bearing sensitizers is seen in many studies concerning fully organic dyes for DSSC [26]. A 60 mV decrease of V_{OC} came as a result of inserting a thiophene π-spacer in **DMA-1** compared to the reference dye. Negligible change was seen when comparing the bithiophene to the single thiophene. However, when we installed a third thiophene another 70 mV drop was observed. As expected, the largest oligothiophene, **DMA-4**, produced the lowest photovoltage at 630 mV. This clearly demonstrate the unfortunate side-effect of elongating oligothiophene π-linkers for organic dyes in DSSCs, as a tremendous 200 mV difference between **DMA-4** and the reference dye was seen.

The obtained IPCE-spectra showed the highest maximum for **DMA-0** (Fig. 8). This is in accordance with one of our previous studies where the highest maximum was obtained for a similar reference dye [20]. As expected, the widest action spectra were found for the longest oligothiophenes **DMA-3** and **DMA-4**. The intensity of the spectra was widely different however, where the maximum of the latter was found at 53% down from 77%. The rigidified bithiophene dye (**DMA-5**) also demonstrated an interesting action spectrum, it was considerably more narrow than the unmodified counterpart **DMA-2**. This shows that rigidifying the π-linker does not necessarily yield an improved light-harvesting ability of the dyes.

The dye loading experiment was carried out through desorption of dyes attached to a TiO_2-electrode, by immersing the electrode in 40 mM tetrabutylammonium hydroxide (TBA(OH)) in THF. The results shown in Table 2 are averages of two separately desorbed electrodes. The homologous series of **DMA-0** – **DMA-4** displayed a higher loading with increasing molecular size. The amount of dye bearing no linker (**DMA-0**) was approximately a third of the quaterthiophene dye (**DMA-4**). This trend is consistent with our findings from one of our previous studies on phenothiazine sensitizers, where incorporation of a furan linker doubled the dye loading compared to the reference without a π-spacer [47]. The reason for this could be that the dyes with π-spacers are able to compete more favorably with the co-adsorbent CDCA for the absorption sites. The large dyes are also more prone to aggregate, which could also be a significant factor that increase the dye loading of the larger dyes.

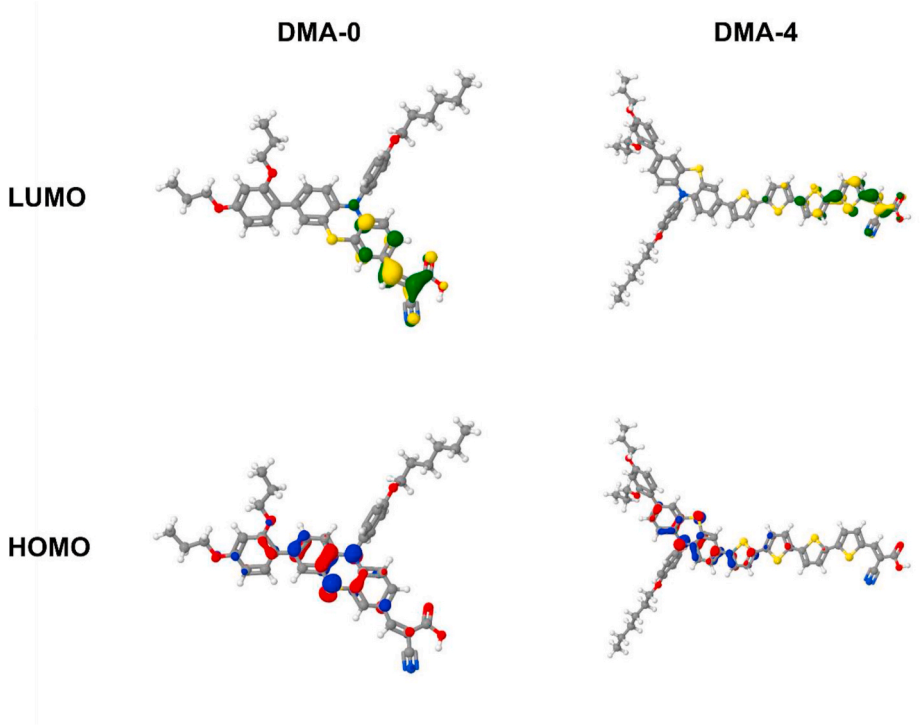

Fig. 6. The frontier orbitals of **DMA-0** and **DMA-4** calculated at the CAM-B3LYP/6-31G(d,p) level.

Table 2
Photovoltaic performance of all dyes under 1 sun AM 1.5G illumination, and from IPCE measurements. Results from dye loading experiments is also included.

Dye	IPCE J_{SC} (mA cm^{-2})[a]	J_{SC} (mA cm^{-2})	V_{OC} (V)	FF	PCE (%)	Dye Loading (10^8 mol cm^{-2})[b]
DMA-0	8.98	10.1 ± 0.2	0.83 ± 0.01	0.68 ± 0.01	5.7 ± 0.2	8.3 ± 0.6
DMA-1	9.75	10.6 ± 0.2	0.77 ± 0.01	0.69 ± 0.02	5.6 ± 0.2	10.1 ± 0.2
DMA-2	9.58	10.9 ± 0.1	0.772 ± 0.002	0.67 ± 0.01	5.6 ± 0.1	22.7 ± 0.9
DMA-3	10.90	11.0 ± 0.1	0.70 ± 0.01	0.68 ± 0.01	5.2 ± 0.1	24.0 ± 0.4
DMA-4	6.91	7.3 ± 0.1[c]	0.628 ± 0.002[c]	0.68 ± 0.04[c]	3.1 ± 0.2[c]	28.1 ± 0.6
DMA-5	8.09	10.3 ± 0.1	0.74 ± 0.01	0.69 ± 0.01	5.3 ± 0.1	16.5 ± 0.3
N719[d]	14.0	13.2	0.70	0.66	6.1	–

[a] Obtained by integration of the IPCE spectrum over the 1 sun AM 1.5 G spectrum.
[b] Values averaged of two desorbed TiO_2-electrodes.
[c] Average values of two cells.
[d] Values from the best-performing device.

2.6. Electrochemical impedance spectroscopy

To investigate the phenomenon of the dropping V_{OC} upon expansion of the π-linker, the dyes **DMA-0 – DMA-4** were analyzed using electrochemical impedance spectroscopy under monochromatic light of 479 nm at different voltages. Impedance data were then used to fit an equivalent circuit (Fig. 9) using non-linear least square fitting with the initial choice of fitting parameters shown in ESI Table S1. The equivalent circuit consists of a transmission line model representing the nanostructured TiO_2 anode, an RC-circuit for the faradaic and non-faradaic processes at the cathode, a finite-diffusion Warburg element for the electrolyte diffusion, and a series resistance for the ohmic resistance.

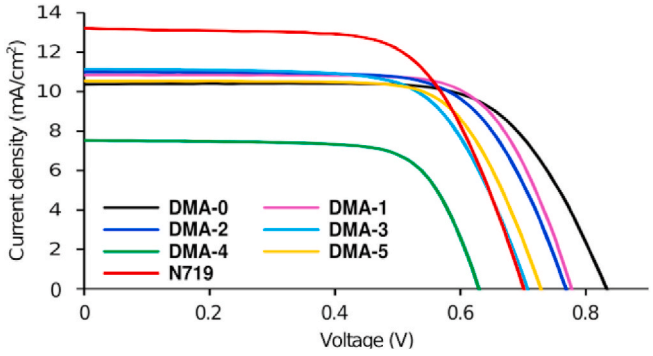

Fig. 7. J-V curves for the best parallel of each dye, obtained under 1 sun AM 1.5G illumination.

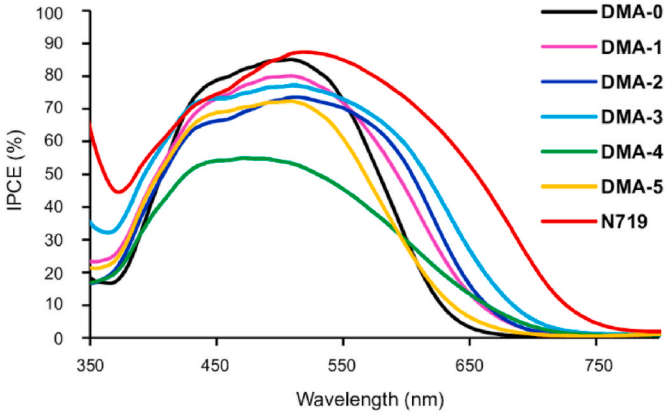

Fig. 8. IPCE spectra of the best performing parallel for each dye.

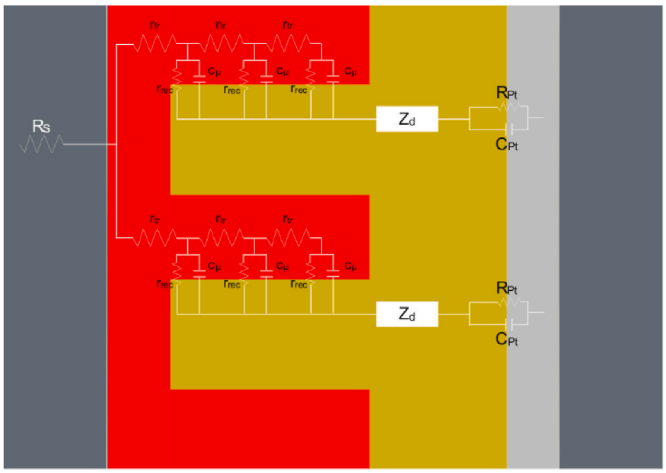

Fig. 9. The equivalent circuit of a dye-sensitized solar cell superimposed on a simple model of the cell itself. The circuit consists of an ohmic series resistance (R_s), a transmission line model with the associated transport resistances (r_{tr}) and recombination resistances (r_{rec}), a finite-diffusion Warburg element (Z_D), and an RC-circuit with a charge transfer resistance (R_{Pt}).

The complete analytical expression for this equivalent circuit is shown in Equation (1).

$$Z = R_s + \frac{R_{RC}}{1 + i\omega R_{RC} C_{RC}} + R_D \frac{\tanh\left[(i\omega/\omega_d)^{1/2}\right]}{(i\omega/\omega_d)^{1/2}} + \left(\frac{R_{tr} R_{rec}}{1 + i\omega/\omega_{rec}}\right)^{1/2} \coth\left[\left(\frac{R_{tr}}{R_{rec}}\right)^{1/2} (1 + i\omega/\omega_{rec})^{1/2}\right] \quad (1)$$

where R_S is the series resistance, R_{RC} and C_{RC} are the resistance and capacitance associated with the RC-circuit at the cathode, R_D is the resistance associated with electrolyte diffusion, R_{tr} is the transport resistance of charges in the semiconductor, and R_{rec} is the recombination resistance between the semiconductor and the electrolyte.

From the fitted impedance parameters, the recombination resistances of the dyes were extracted, and are shown as a function of applied voltage in (Fig. 10a). The results clearly show that the recombination resistance decreases with increasingly sized oligothiophene π-spacers. This might be explained by the higher number of sulfur atoms, causing a higher probability of sulfur-iodine interaction, which in turn promote recombination across the TiO_2-electrolyte interface. Alternatively, it could be caused by clustering/domain formation of aggregated rod-like dyes, giving the electrolyte access to the TiO_2. In any case, the increase in recombination is contributing to lowering the Fermi level of TiO_2, thus reducing the V_{OC} of the devices [48].

The impedance data obtained was also fitted to generate a *J-V* curve as explained by Fabregat-Santiago et al. [49] The fitted curves and the obtained J-V curves for **DMA-0** and **DMA-4** are shown in (Fig. 10b) and illustrates how **DMA-0** displayed a near perfect overlap, while discrepancies were present for **DMA-4**. This suggest that for **DMA-0** a normal DSSC-behavior was seen where the major resistance element is the recombination. The deviation seen for **DMA-4** is indicative of Gerischer behavior where transport resistance is larger than recombination resistance [50]. This further supports the claim that the voltage drops associated with large oligothiophene π-spacers are caused by a facilitation of recombination. The fitted curves and obtained J-V curves for the homologous series **DMA-0 – DMA-4** (ESI Fig. S6) showed overlapping curves for all dyes except **DMA-4**.

3. Conclusion

The effect of five different thiophene/oligothiophene π-spacers has been investigated and compared to the π-linker free analogue. The dye without π-linker produced the highest photovoltage, while the sensitizers containing mono- and bithiophene produced higher photocurrents without too detrimental voltage drops. Because of this, the PCE-values of **DMA-0** – **DMA-2** were quite similar at 5.6–5.7%. The terthiophene dye (**DMA-3**) produced the highest photocurrent, alas the voltage drops associated with larger oligothiophenes led to a significant drop in PCE for this dye. Finally, the dye containing the quaterthiophene π-spacer produced the lowest efficiency out of the dyes tested. Further examination of the dye (**DMA-4**) using impedance measurements showed a Gerischer behavior of the device. In the author's opinion the opportunities that **DMA-3** presents has not yet been fully explored. For instance, modifying the π-spacer with steric functionalities could help preventing the electrolyte from reaching the TiO_2 surface. Such a modification should allow for the dye's promising charge generation to not be weighed down by poor photovoltages.

Overall, we conclude that incorporating thiophene, bithiophene or terthiophene in π-spacers of phenothiazine dyes for DSSC gives no added benefits in terms of PCE, while a significant drop in efficiency is seen for the quaterthiophene containing dye.

4. Experimental

4.1. Materials and reagents

All reactions were performed under inert N_2-atmosphere. The chemicals used were all purchased from Sigma-Aldrich, apart from 2,2':5',2''-Terthiophene which was purchased from abcr GmbH. A full account of the synthetic procedures is given in the ESI.

4.2. Computational details

Initial 3D geometries of the molecules were generated using

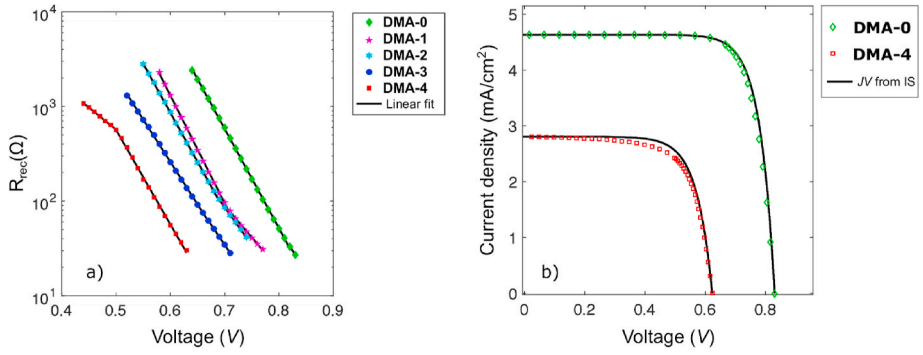

Fig. 10. a) The recombination resistances of the dyes, obtained from EIS under monochromatic light, plotted against applied voltage. b) J-V curves obtained for **DMA-0** (◊) and **DMA-4** (□) under monochromatic light of 479 nm and J-V curves (–) recreated from impedance spectroscopy data.

OpenBabel [51] followed by a semiempirical PM6 Hamiltonian level optimization using MOPAC [52]. Further optimization in solvent (dichloromethane) was carried out using the B3LYP functional and the 6-31G(d,p) basis set. Solvent effects were considered using the using the conductor-like polarizable continuum model. Subsequently, time-dependent density functional theory (TD-DFT) calculations were performed at the CAM-B3LYP/6-31G(d,p) level of theory. The DFT computations were carried out using Gaussian 09 [45].

4.3. Analytical instruments

^{1}H and ^{13}C NMR was performed using either a BRUKER 400 MHz or 600 MHz magnet, the spectra obtained are calibrated against TMS (0 ppm) in $CDCl_3$ or against the residual solvent peak of DMSO-d_6 (2.50/39.52 ppm) or THF-d_8 (3.58/67.57 ppm). The IR-spectra are obtained using a BRUKER Alpha Eco-ATR FTIR spectrometer, the data is reported with wavenumber and according intensity of signal. Mass determination was performed by MS-analysis in positive ionization mode on a Synapt G2-S Q-TOF-instrument for Waters, the samples were ionized by an ASAP-probe (APCI) without prior chromatographic separation. UV–Vis spectroscopy was performed using a Hitachi U-1900 spectrometer, and photoluminescence characterization was carried out on an Edinburgh Instruments FS5-spectrofluorometer.

4.4. Fabrication of dye-sensitized solar cells

The anodes were prepared from FTO glass (NSG10, Nippon Sheet Glass), which was first cleaned in a Deconex 21-solution (2 g/L) under sonication for 45 min. Next the FTO was treated with UV/O_3 (Novascan PSD PRO-UV T6) for 15 min. Immersion of the glass in aqueous $TiCl_4$-solution (40 mM) at 70 °C for 2 × 45 min followed by rinsing with deionized water and ethanol was carried out to deposit a blocking layer on the FTO-sample. Pastes of TiO_2 were screen printed onto the FTO (mesh count 54, thread diameter 64 mm, area 0.2826 cm^2), first two active layers (18NR-T, Dyesol) were printed, with 5 min heating on a hotplate at 125 °C after each layer. A scattering layer (WER2-O, Dyesol) was ultimately printed, and the TiO_2 was sintered in a programmable furnace (Nabertherm LT 9/12) at set temperatures of 125, 250, 325, 450, and 500 °C for 5, 5, 5, 15, and 15 min with a ramping time of 10 min. Upon cooling to room temperature, the anodes were treated with aq. $TiCl_4$ as described earlier. Before staining the electrodes were annealed at 500 °C for 30 min, using a hot air gun.

The counter electrodes were prepared from TEC10 FTO glass supplied by Sigma Aldrich. Holes were drilled into the electrodes from the FTO-side using a diamond drill bit, this procedure was carried out under water. The glass plates were then cleaned using Deconex 21 (aq., 2 g/L), deionized water, ethanol, and acetone, in an ultrasonic bath for 15 min for each. A solution of H_2PtCl_6 (10 mM in 2-propanol) was dropcast (5 μL/cm^2) on the FTO before heating at 400 °C for 15 min with a hot air gun formed the catalytic layer of Pt.

The photoanodes were placed in the dye bath while still holding ~80 °C from the annealing-procedure and stored at 30 °C for 15 h. The dye baths were prepared using a mixture of acetonitrile and THF (43/57, v/v) to make a solution of dye and co-adsorbent CDCA, at concentrations of 0.5 mM and 5 mM respectively. The staining of the reference **N719** was done similarly, but the solvent used was in this case ethanol. After the staining of the electrodes, they were rinsed in acetonitrile for 2 min, then sealed to the counter electrode using Surlyn (25 μm, Solaronix) in a drybox. A 4 × 20 s treatment of the cell using a 50 W PTC heat element was sufficient to seal the cells. The electrolyte was vacuum backfilled into the device, the filling-hole was sealed with Surlyn and a glass cover disk, then to complete the devices the exposed electrodes were painted with silver conducting paint (Electrolube, SCP). The electrolyte employed was the A6141 electrolyte, consisting of butylmethylimidazolium iodide (0.60 M), I_2 (0.03 M), guanidinium thiocyanate (0.1 M), and *t*-butylpyridine (0.50 M) dissolved in acetonitrile/valeronitrile (85/15, v/v) [53].

The devices used in the impedance measurements were prepared in a similar manner, the only differences being that the FTO glass for the photoanodes were TEC10 from Sigma-Aldrich and the gasket employed was thicker (60 μm, Solaronix).

4.5. Device characterization

J-V curves were obtained under 1 sun illumination AM 1.5G illumination provided by a Sciencetech SP300B solar simulator, calibrated with a Newport Reference Cell (91150 V), connected to a Keithley 2450 SourceMeter. A mask with an active area of 0.238 cm^2 was used on all the *J-V* measurements. IPCE measurements were carried out using a halogen lamp (Ocean Optics HL-2000) and a monochromator (Spectral Products CM110) connected to the Keithley 2450. The devices and the reference photodiode (Thorlabs, FDS100-CAL) were covered with a mask with a size of 0.049 cm^2.

The electrochemical impedance properties were measured in a light-exclusion box containing a Zahner CIMPS QE/IPCE TLS03 tunable light source. The light source was connected to a Zahner XPOT potentiostat, the devices were connected to a Zahner IM6ex potentiostat, both potentiostats were controlled by the Thales software. EIS was performed both in dark conditions and under constant illumination at wavelength 479 nm with an intensity of 12.6 mW/cm^2. For both cases the voltage across the cells was oscillating with an amplitude of 10 mV over a 100 mHz–100 kHz frequency range. The measurements were distributed logarithmically over this range with 8 measurements per decade for frequencies higher than 66 Hz and 3 measurements per decade for frequencies lower than 66 Hz. The results above 66 Hz were also averaged over 20 measurements for every frequency while the results below 66 Hz were averaged over 2 measurements per frequency. The oscillating voltage across the DSSCs had an applied DC-bias during the measurements which was decreased by 10 mV between measurements starting at the open circuit voltage of the cells. All DSSCs were measured 20 times each, with the DC-bias voltage as the variable.

Credit authorship contribution statement

David Moe Almenningen: Investigation, Methodology, Conceptualization, Writing – Original Draft, Visualization. **Henrik Erring Hansen:** Investigation, Methodology, Writing – Review & Editing, Visualization. **Martin Furru Vold:** Investigation. **Audun Formo Buene:** Methodology, Writing – Review & Editing, Visualization. **Vishwesh Venkatraman**: Investigation, Visualization. **Svein Sunde:** Supervision, Writing – Review & Editing. **Bård Helge Hoff:** Supervision, Writing – Review & Editing. **Odd Reidar Gautun:** Supervision, Conceptualization, Writing – Review & Editing.

One additional author has been included for his help with DFT calculations (Dr Vishwesh Venkatraman).

Declaration of competing interest

The authors declare that they have no known competing financial interests or personal relationships that could have appeared to influence the work reported in this paper.

Acknowledgements

The authors acknowledge staff engineer Roger Aarvik and Ph.D. Susana Villa Gonzalez for their technical and mass spectrometry contributions. The support from the Research Council of Norway to the Norwegian NMR Platform (project number 226244/F50) is much appreciated. The Research Council of Norway is acknowledged for the support to the Norwegian Micro- and Nano-Fabrication Facility, NorFab, project number 245963/F50. VV thanks support from grant (Grant No. 262152) from the Research Council of Norway.

Appendix A. Supplementary data

Supplementary data to this article can be found online at https://doi.org/10.1016/j.dyepig.2020.108951.

References

[1] O'Regan B, Grätzel M. A low-cost, high-efficiency solar cell based on dye-sensitized colloidal TiO2 films. Nature 1991;353(6346):737–40.
[2] Snaith HJ, Schmidt-Mende L. Advances in liquid-electrolyte and solid-state dye-sensitized solar cells. Adv Mater 2007;19(20):3187–200.
[3] Yun MJ, Cha SI, Seo SH, Lee DY. Highly flexible dye-sensitized solar cells produced by sewing textile electrodes on cloth. Sci Rep 2014;4:5322.
[4] Cao Y, Liu Y, Zakeeruddin SM, Hagfeldt A, Grätzel M. Direct contact of selective charge extraction layers enables high-efficiency molecular photovoltaics. Joule 2018;2(6):1108–17.
[5] Hardin BE, Snaith HJ, McGehee MD. The renaissance of dye-sensitized solar cells. Nat Photon 2012;6:162.
[6] Hagberg DP, Marinado T, Karlsson KM, Nonomura K, Qin P, Boschloo G, et al. Tuning the HOMO and LUMO energy levels of organic chromophores for dye sensitized solar cells. J Org Chem 2007;72(25):9550–6.
[7] Genin E, Hugues V, Clermont G, Herbivo C, Castro MCR, Comel A, et al. Fluorescence and two-photon absorption of push–pull aryl(bi)thiophenes: structure–property relationships. Photochem Photobiol Sci 2012;11(11):1756–66.
[8] Kulhánek J, Bureš F, Pytela O, Mikysek T, Ludvík J, Růžička A. Push-pull molecules with a systematically extended π-conjugated system featuring 4,5-dicyanoimidazole. Dyes Pigments 2010;85(1):57–65.
[9] Kulhánek J, Bureš F, Wojciechowski A, Makowska-Janusik M, Gondek E, Kityk IV. Optical operation by chromophores featuring 4,5-dicyanoimidazole embedded within poly(methyl methacrylate) matrices. J Phys Chem 2010;114(35):9440–6.
[10] Stiegman AE, Graham E, Perry KJ, Khundkar LR, Cheng LT, Perry JW. The electronic structure and second-order nonlinear optical properties of donor-acceptor acetylenes: a detailed investigation of structure-property relationships. J Am Chem Soc 1991;113(20):7658–66.
[11] Bureš F. Fundamental aspects of property tuning in push–pull molecules. RSC Adv 2014;4(102):58826–51.
[12] Hagfeldt A, Boschloo G, Sun L, Kloo L, Pettersson H. Dye-sensitized solar cells. Chem Rev 2010;110(11):6595–663.
[13] Joly D, Pellejà L, Narbey S, Oswald F, Chiron J, Clifford JN, et al. A robust organic dye for dye sensitized solar cells based on iodine/iodide electrolytes combining high efficiency and outstanding stability. Sci Rep 2014;4:4033.
[14] Tsao HN, Burschka J, Yi C, Kessler F, Nazeeruddin MK, Grätzel M. Influence of the interfacial charge-transfer resistance at the counter electrode in dye-sensitized solar cells employing cobalt redox shuttles. Energy Environ Sci 2011;4(12):4921–4.
[15] Ellis H, Eriksson SK, Feldt SM, Gabrielsson E, Lohse PW, Lindblad R, et al. Linker unit modification of triphenylamine-based organic dyes for efficient cobalt mediated dye-sensitized solar cells. J Phys Chem C 2013;117(41):21029–36.
[16] Yao Z, Wu H, Ren Y, Guo Y, Wang P. A structurally simple perylene dye with ethynylbenzothiadiazole-benzoic acid as the electron acceptor achieves an over 10% power conversion efficiency. Energy Environ Sci 2015;8(5):1438–42.
[17] Yao Z, Yang L, Cai Y, Yan C, Zhang M, Cai N, et al. Rigidifying the π-linker to enhance light absorption of organic dye-sensitized solar cells and influences on charge transfer dynamics. J Phys Chem C 2014;118(6):2977–86.
[18] Hao Y, Saygili Y, Cong J, Eriksson A, Yang W, Zhang J, et al. Novel blue organic dye for dye-sensitized solar cells achieving high efficiency in cobalt-based electrolytes and by Co-sensitization. ACS Appl Mater Interfaces 2016;8(48):32797–804.
[19] Kakiage K, Aoyama Y, Yano T, Oya K, Fujisawa J-i, Hanaya M. Highly-efficient dye-sensitized solar cells with collaborative sensitization by silyl-anchor and carboxy-anchor dyes. Chem Commun 2015;51(88):15894–7.
[20] Buene AF, Uggerud N, Economopoulos SP, Gautun OR, Hoff BH. Effect of π-linkers on phenothiazine sensitizers for dye-sensitized solar cells. Dyes Pigments 2018;151:263–71.
[21] Iqbal Z, Wu W-Q, Huang Z-S, Wang L, Kuang D-B, Meier H, et al. Trilateral π-conjugation extensions of phenothiazine-based dyes enhance the photovoltaic performance of the dye-sensitized solar cells. Dyes Pigments 2016;124:63–71.
[22] Hara K, Wang Z-S, Sato T, Furube A, Katoh R, Sugihara H, et al. Oligothiophene-containing coumarin dyes for efficient dye-sensitized solar cells. J Phys Chem B 2005;109(32):15476–82.
[23] Gao H-H, Qian X, Chang W-Y, Wang S-S, Zhu Y-Z, Zheng J-Y. Oligothiophene-linked D–π–A type phenothiazine dyes for dye-sensitized solar cells. J Power Sources 2016;307:866–74.
[24] Qian X, Zhu Y-Z, Chang W-Y, Song J, Pan B, Lu L, et al. Benzo[a]carbazole-Based donor−π–acceptor type organic dyes for highly efficient dye-sensitized solar cells. ACS Appl Mater Interfaces 2015;7(17):9015–22.
[25] Li R, Lv X, Shi D, Zhou D, Cheng Y, Zhang G, et al. Dye-sensitized solar cells based on organic sensitizers with different conjugated linkers: furan, bifuran, thiophene, bithiophene, selenophene, and biselenophene. J Phys Chem C 2009;113(17):7469–79.
[26] Liu J, Li R, Si X, Zhou D, Shi Y, Wang Y, et al. Oligothiophene dye-sensitized solar cells. Energy Environ Sci 2010;3(12):1924–8.
[27] Ronca E, Pastore M, Belpassi L, Tarantelli F, De Angelis F. Influence of the dye molecular structure on the TiO2 conduction band in dye-sensitized solar cells: disentangling charge transfer and electrostatic effects. Energy Environ Sci 2013;6(1):183–93.
[28] Zhang M, Liu J, Wang Y, Zhou D, Wang P. Redox couple related influences of π-conjugation extension in organic dye-sensitized mesoscopic solar cells. Chem Sci 2011;2(7):1401–6.
[29] Rühle S, Greenshtein M, Chen SG, Merson A, Pizem H, Sukenik CS, et al. Molecular adjustment of the electronic properties of nanoporous electrodes in dye-sensitized solar cells. J Phys Chem B 2005;109(40):18907–13.
[30] Eom YK, Kang SH, Choi IT, Kim E, Kim J, Ju MJ, et al. New thieno[3,2-b][1]benzothiophene-based organic sensitizers containing π-extended thiophene spacers for efficient dye-sensitized solar cells. RSC Adv 2015;5(98):80859–70.
[31] Kakiage K, Aoyama Y, Yano T, Otsuka T, Kyomen T, Unno M, et al. An achievement of over 12 percent efficiency in an organic dye-sensitized solar cell. Chem Commun 2014;50(48):6379–81.
[32] Hua Y, Lin Lee LT, Zhang C, Zhao J, Chen T, Wong W-Y, et al. Co-sensitization of 3D bulky phenothiazine-cored photosensitizers with planar squaraine dyes for efficient dye-sensitized solar cells. J Mater Chem 2015;3(26):13848–55.
[33] Lin RY-Y, Wu F-L, Li C-T, Chen P-Y, Ho K-C, Lin JT. High-performance aqueous/organic dye-sensitized solar cells based on sensitizers containing triethylene oxide methyl ether. ChemSusChem 2015;8(15):2503–13.
[34] Hagberg DP, Jiang X, Gabrielsson E, Linder M, Marinado T, Brinck T, et al. Symmetric and unsymmetric donor functionalization. comparing structural and spectral benefits of chromophores for dye-sensitized solar cells. J Mater Chem 2009;19(39):7232–8.
[35] Blouin N, Berny S, Jackson EA, Richter H, He F. Cyclohexadiene fullerene derivatives. 2014. US.
[36] Seo Y-H, Lee W-H, Park J-H, Bae C, Hong Y, Park J-W, et al. Side-chain effects on phenothiazine-based donor–acceptor copolymer properties in organic photovoltaic devices. J Polym Sci, Part A: Polym Chem 2012;50(4):649–58.
[37] Bejan A, Shova S, Damaceanu M-D, Simionescu BC, Marin L. Structure-directed functional properties of phenothiazine brominated dyes: morphology and photophysical and electrochemical properties. Cryst Growth Des 2016;16(7):3716–30.
[38] Billingsley KL, Buchwald SL. An improved system for the palladium-catalyzed borylation of aryl halides with pinacol borane. J Org Chem 2008;73(14):5589–91.
[39] Tian H, Yang X, Chen R, Zhang R, Hagfeldt A, Sun L. Effect of different dye baths and dye-structures on the performance of dye-sensitized solar cells based on triphenylamine dyes. J Phys Chem C 2008;112(29):11023–33.
[40] Dentani T, Kubota Y, Funabiki K, Jin J, Yoshida T, Minoura H, et al. Novel thiophene-conjugated indoline dyes for zinc oxide solar cells. New J Chem 2009;33(1):93–101.
[41] Pavlishchuk VV, Addison AW. Conversion constants for redox potentials measured versus different reference electrodes in acetonitrile solutions at 25°C. Inorg Chim Acta 2000;298(1):97–102.
[42] Kim SH, Kim HW, Sakong C, Namgoong J, Park SW, Ko MJ, et al. Effect of five-membered heteroaromatic linkers to the performance of phenothiazine-based dye-sensitized solar cells. Org Lett 2011;13(21):5784–7.
[43] Tian H, Yang X, Chen R, Pan Y, Li L, Hagfeldt A, et al. Phenothiazine derivatives for efficient organic dye-sensitized solar cells. Chem Commun 2007;(36):3741–3.
[44] Saygili Y, Söderberg M, Pellet N, Giordano F, Cao Y, Muñoz-García AB, et al. Copper bipyridyl redox mediators for dye-sensitized solar cells with high photovoltage. J Am Chem Soc 2016;138(45):15087–96.
[45] Frisch MJ, et al. Gaussian 09, revision b.01. Wallingford CT: Gaussian, Inc.; 2010.
[46] Christians JA, Manser JS, Kamat PV. Best practices in perovskite solar cell efficiency measurements. Avoiding the error of making bad cells look good. J Phys Chem Lett 2015;6(5):852–7.
[47] Buene AF, Boholm N, Hagfeldt A, Hoff B. Effect of furan π-spacer and triethylene oxide methyl ether substituents on performance of phenothiazine sensitizers in dye-sensitized solar cells. New J Chem 2019;43(24):9403–10.
[48] Pazoki M, Cappel UB, Johansson EMJ, Hagfeldt A, Boschloo G. Characterization techniques for dye-sensitized solar cells. Energy Environ Sci 2017;10(3):672–709.
[49] Fabregat-Santiago F, Bisquert J, Palomares E, Otero L, Kuang D, Zakeeruddin SM, et al. Correlation between photovoltaic performance and impedance spectroscopy of dye-sensitized solar cells based on ionic liquids. J Phys Chem C 2007;111(17):6550–60.
[50] Fabregat-Santiago F, Garcia-Belmonte G, Mora-Seró I, Bisquert J. Characterization of nanostructured hybrid and organic solar cells by impedance spectroscopy. Phys Chem Chem Phys 2011;13(20):9083–118.
[51] O'Boyle NM, Banck M, James CA, Morley C, Vandermeersch T, Hutchison GR. Open Babel: an open chemical toolbox. J Cheminf 2011;3(1):33.
[52] Stewart JJP. MOPAC2016. Colorado Springs, CO, USA: Stewart Computational Chemistry; 2016.
[53] Nazeeruddin MK, De Angelis F, Fantacci S, Selloni A, Viscardi G, Liska P, et al. Combined experimental and DFT-TDDFT computational study of photoelectrochemical cell ruthenium sensitizers. J Am Chem Soc 2005;127(48):16835–47.